Reducing the diffraction artifacts while implementing a phase function on a spatial light modulator

Céline Benoit-Pasanau, François Goudail, Pierre Chavel, Jean-Paul Cano, Jérôme Ballet

Reducing the diffraction artifacts while implementing a phase function on a spatial light modulator

Céline Benoît-Pasanau,[1,2] François Goudail,[1,*] Pierre Chavel,[1] Jean-Paul Cano,[2] and Jérôme Ballet[2]

[1]Laboratoire Charles Fabry de l'Institut d'Optique, CNRS, Université Paris-Sud, Campus Polytechnique, RD 128, 91127 Palaiseau, France

[2]Essilor International, Rue Pierre et Marie Curie, 31670 Labège, France

*Corresponding author: francois.goudail@institutoptique.fr

Received 10 September 2010; revised 23 November 2010; accepted 5 December 2010; posted 6 December 2010 (Doc. ID 134933); published 27 January 2011

Spatial light modulators are often used to implement phase modulation. Since they are pixelated, the phase function is usually approximated by a regularly sampled piecewise constant function, and the periodicity of the pixel sampling generates annoying diffraction peaks. We theoretically investigate two pixelation techniques: the isophase method and a new nonperiodic method derived from the Voronoi tessellation technique. We show that, for a suitable choice of parameters, the diffraction peaks disappear and are replaced by a smoothly varying halo. We illustrate the potential of these two techniques for implementing a lens function and wavefront correction. © 2011 Optical Society of America

OCIS codes: 050.1940, 230.6120.

1. Introduction

Spatial light modulators (SLMs) are components that can be used to implement spatially varying phase modulations [1,2]. They are useful for implementing optical functions in imaging or wavefront correction [3,4]. Their aperture is divided into small cells, called pixels, that are usually square- or rectangle-shaped and distributed periodically. Because of this periodic arrangement, the diffraction patterns are affected by artifacts that take the form of periodically distributed diffraction peaks in the Fourier plane. For example, it has been shown that pixelated lenses displayed on an SLM can produce a large number of equally intense replica images [1,5–8]. The shape and intensity of the diffraction orders produced by those components, responsible for a multiple imaging effect, have been investigated in several earlier publications [5–8]. Our objective in this paper is to reduce these diffraction peaks by introducing disorder in the regular square-shaped structure of the modulator. We study and compare two ways to implement this idea: the so-called isophases and the Voronoi diagrams. The Voronoi technique already showed its capability to reduce diffraction peaks when only the diffraction by the walls between the pixels is taken into account [9]. In Ref. [9], we considered periodic or nonperiodic arrangements of pixels but with one and the same uniform phase in all pixels. In the present work, we extend the investigation to the practically more important case where a phase function is encoded onto the SLM. Therefore, even with a periodic arrangement of the pixels, the SLM transmittance is not a periodic function. The periodicity nevertheless creates diffraction peaks. Suitable nonperiodic arrangements will be shown to circumvent the problem. In the present work, as opposed to Ref. [9], the walls between pixels are neglected, which means they are considered infinitely thin.

In this paper, our main focus will be on the design of structures with desired diffraction properties, and we will not address the issue of their practical realization.

The paper is organized as follows. In Section 2, we introduce two nonperiodic pixelation techniques, and

0003-6935/11/040509-10$15.00/0

we illustrate their performances by considering the implementation of a pixelated lens. In Section 3, we compare their capacities for the correction of different types of optical aberrations, and we finally conclude in Section 4.

2. Comparison of Different Pixelation Methods

In order to reduce the diffraction peaks, our idea is to introduce disorder in a regular SLM. In this section, we investigate two different techniques to implement this idea. We compare their performances by considering the implementation of a pixelated lens of focal length f, which, in the Fresnel approximation, corresponds to the following phase function:

$$\varphi_d(x,y) = \frac{\pi}{\lambda f}(x^2 + y^2). \tag{1}$$

A. Pixelation of a Phase Function

Let us denote $\varphi_{\text{ideal}}(x,y)$ the continuous ideal phase that we want to implement. Pixelation consists in approximating $\varphi_{\text{ideal}}(x,y)$ with a piecewise constant function, so that each cell of the SLM has a constant phase value φ_p, chosen to minimize the quantity of diffracted light. Throughout this investigation, we assume that the difference between $\varphi_{\text{ideal}}(x,y)$ and φ_p remains moderate, so that the effect of pixelation can be analyzed based on an expansion of their difference. For a given pixel covering the domain D, the value of φ_p that minimizes the diffraction losses is such that the square deviation σ_Φ^2 with $\varphi_{\text{ideal}}(x,y)$ is minimum (Maréchal criterion [10]):

$$\sigma_\Phi^2 = \iint_D (\varphi_{\text{ideal}}(x,y) - \varphi_p)^2 \mathrm{d}x\mathrm{d}y. \tag{2}$$

We look for the phase φ_p that minimize σ_Φ^2, which means

$$\frac{\partial}{\partial \varphi_p} \iint_D (\varphi_{\text{ideal}}(x,y) - \varphi_p)^2 \mathrm{d}x\mathrm{d}y = 0. \tag{3}$$

If we call s the surface of a cell, one gets

$$\varphi_p = \frac{1}{s} \iint_D \varphi_{\text{ideal}}(x,y) \mathrm{d}x\mathrm{d}y. \tag{4}$$

As a result, we will associate to each cell the average of the ideal phase function over its area.

As an example, let us consider the case of a lens whose phase function is defined by Eq. (1) and of focal length $f = 2\,\text{m}$, implemented on an SLM with square-shaped pixels whose pixel pitch is equal to d. We assume that it is illuminated by a monochromatic plane wave of wavelength $\lambda = 0.5\,\mu\text{m}$, propagating parallel to the optical axis, and we observe the distribution of light intensity in the focal plane. The modulator's aperture is a disc of diameter 4 mm. Let (ξ,η) be the coordinates of a point in the focal plane; we call relative intensity $E(\xi,\eta)$ the ratio given by

$$E(\xi,\eta) = \frac{I(\xi,\eta)}{I_{\text{airy}}}, \tag{5}$$

where $I(\xi,\eta)$ is the intensity diffracted by the pixelated lens, and I_{airy} is the intensity in the central lobe of the Airy pattern that would be generated by the clear aperture in the same focal plane. As a result, the Strehl ratio S [11] can be defined as

$$S = \max(E(\xi,\eta)). \tag{6}$$

In Fig. 1, we have considered an SLM with square-shaped pixels. The pixel pitch is equal to $d = 100\,\mu\text{m}$. In Fig. 1(c), we have represented the relative intensity $E(\xi,\eta)$ obtained with the SLM structure of Fig. 1(b), as well as a cross section in the horizontal direction in Fig. 1(d). To account for the spatial integration by the sensor, we have spatially averaged the relative intensity by a convolution with a rectangular function of width 1 arc min. As a result of this averaging, the observed diffraction peaks do not have the aspect of the derivative of the Bessel function $\frac{J_1(X)}{X}$, as described in [8]. Figures 1(c) and 1(d) illustrate the well-known fact that the intensity distribution in the focal plane of a square-shaped modulator consists of a zeroth order, located at zero diffraction angle [highlighted by a circle on Fig. 1(d)] and of higher orders (peaks) periodically distributed with an angular period equal to λ/d. For example, the first-order peak is highlighted by a dotted circle on Fig. 1(d). As the focal length of the pixelated lens decreases, the diffraction peaks create replica lens patterns which are responsible for a multiple imaging effect [1,5–8]. In this paper, we will consider that the focal length and sampling rates are such that this multiple imaging effect is avoided. In Subsections 2.B and 2.C, we investigate two ways of reducing these diffraction peaks.

B. Pixelation by Isophases

The first method we choose to investigate is the pixelation by isophases. To begin with, we shall present its principle and next illustrate its application to a pixelated lens.

The pixelation principle is explained in Fig. 2. The phase function is considered as a function $z = \varphi(x,y)$ and is sliced by equally spaced horizontal planes $z = 2k\pi\gamma$, where k is an integer and γ is a real number. The projections on the SLM of the intersections between each of these planes and the phase function define the shapes of the isophase cells. For a better understanding of the repartition of the cells, we represent in Fig. 3 the pixelation by isophases for a lens with $f = 2\,\text{m}$ for $\gamma = 0.1$. Each cell is an annulus with a given width. In our case, the annuli draw closer when the slope of the phase function increases. As a result, there is no periodicity in the pixelation, and higher-order diffraction peaks do not exist.

The main issue is to choose the value of γ. Of course, the smaller γ is, the better, since it will lead to

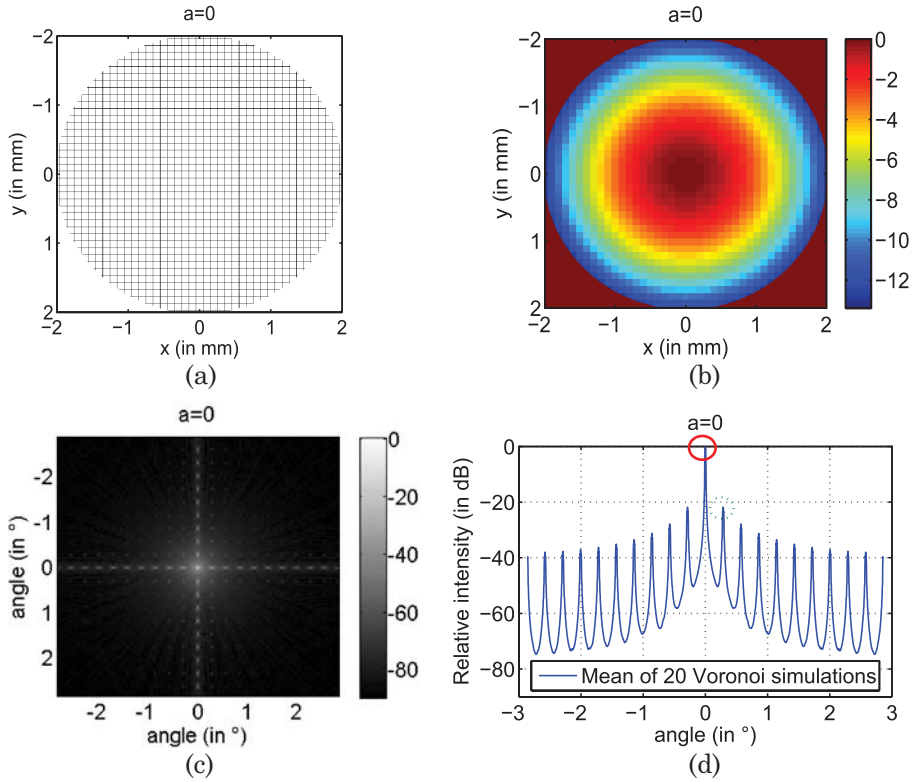

Fig. 1. (Color online) SLM with square-shaped pixel, pixel pitch $d = 100\,\mu$m. Pupil diameter of 4 mm. (a) Walls only. (b) Implementation of a pixelated lens of focal length $f = 2$ m. (c) Diffracted intensity by the pixelated SLM. (d) Corresponding cross section of (c) in the horizontal direction.

a better approximation of the ideal phase. However, there is a lower limit due to technological reasons: the thinnest annuli must be technologically realizable by using the appropriate lithographic equipment. As a compromise, we consider here that no isophase annulus thinner than some minimal distance $d_{\min}$ will be authorized. When γ is very small, as in Fig. 4(a) with $\gamma = 0.05$, most cells have the minimal size $d_{\min}$. This situation is equivalent to a periodic pixelation and produces diffraction peaks. When γ is larger, as in Fig. 4(c) with $\gamma = 0.15$, the distance between the isophases is larger and undersampling effects may arise. There is thus an optimum value for γ that reduces the diffracted relative intensity at angle $\lambda/d_{\min}$ (first-order peak). It corresponds to a phase profile where the distances between the isophases are different from another, with few cells of size $d_{\min}$ [see Fig. 4(b)]. For our simulations of a lens function of focal length $f = 2$ m, we have chosen $d_{\min} = 50\,\mu$m and $\gamma = 0.1$.

Let us now compare the isophase pixelation with the regular square-shaped one of period $d = 100\,\mu$m while implementing a pixelated lens. In Fig. 5, we have plotted a horizontal section of the diffraction relative intensities of both pixelation techniques. We notice that the angular distribution of the relative intensity is more uniform with the isophases than with the regular grid. Instead of diffraction peaks, we have a smoothly varying halo. Moreover, outside the zero-order peak, the maximum of the diffracted

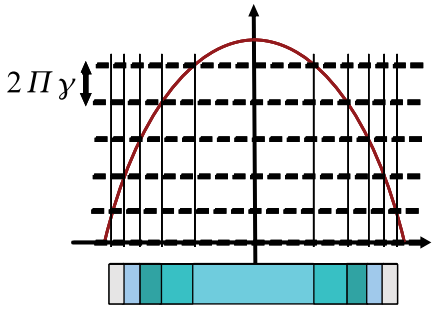

Fig. 2. (Color online) Principle of the pixelation by isophases. The phase function is sliced by equally spaced horizontal planes $z = 2k\pi\gamma$ (k, integer, and γ, a real number).

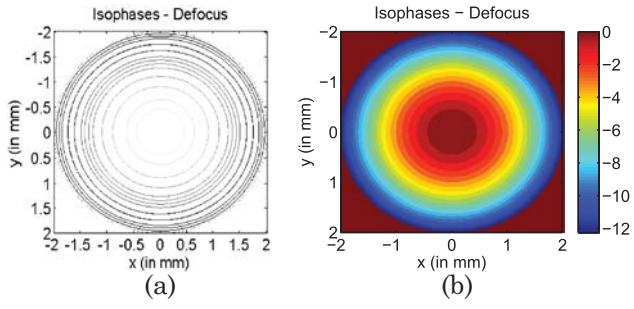

Fig. 3. (Color online) Lens of focal length $f = 2$ m encoded in an isophase modulator. (a) Isophases only. (b) Phase in the modulator. Pupil of 4 mm diameter.

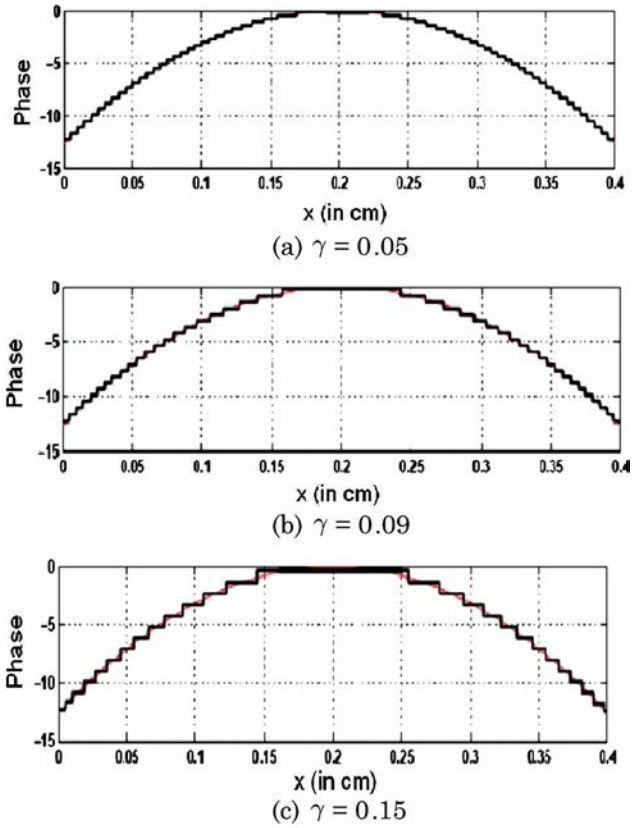

Fig. 4. Different phase profiles of the pixelated lens of focal length $f = 2\,\mathrm{m}$ encoded in different isophase modulators. (a) $\gamma = 0.05$, (b) $\gamma = 0.09$, and (c) $\gamma = 0.15$.

intensity is always inferior to −50 dB for the isophases. This residual halo is less annoying than diffraction peaks for a human observer or the automatic analysis of the images.

We can see in Table 1 that the Strehl ratio [see Eq. (6)] obtained with the isophases is better than the one obtained with the regular square grid. In Table 1, we have also represented G, the difference

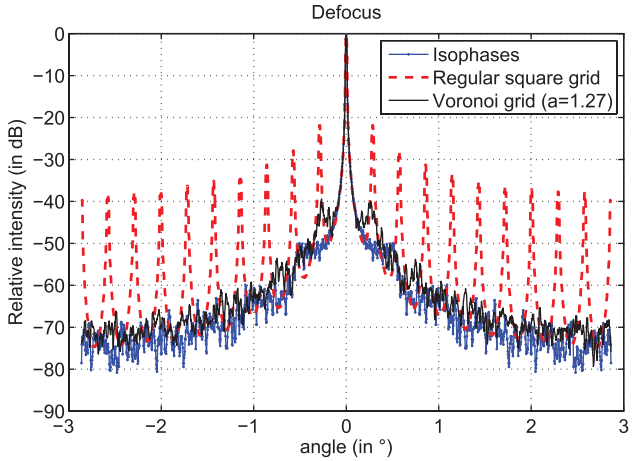

Fig. 5. (Color online) Lens of focal length $f = 2\,\mathrm{m}$. Comparison of the horizontal sections of the diffracted intensity by a regular square grid ($d = 100\,\mu\mathrm{m}$), an optimal Voronoi grid ($a = 1.27$) and by isophases.

Table 1. Lens of Focal Length $f = 2\,\mathrm{m}$[a]

	S	G
Square grid	0.94	-
Isophases	0.97	28
Voronoi ($d = 100\,\mu\mathrm{m}$)	0.92	18

[a]Strehl ratios S and difference in decibels, denoted G, between the first-order peak of the square grid and the maximum of the halo of the studied pixelated grid.

in decibels between the relative intensity of the first-order peak of the square grid and the relative intensity of the maximum of the halo created by the isophases: it is equal to 28 dB. The isophase technique is thus efficient, but the shape of the cells is specific to a given phase function. So, in Subsection 2.C we propose another technique whose advantage is to lead to a pixelation pattern that is independent of the implemented phase function.

C. Pixelation by Voronoi Diagrams

A Voronoi diagram [12] is a partition of the plane built on n generating points p_i, $i \in [1, N]$. The partition consists of convex polygons such that each polygon contains exactly one generating point p_i and every point in a given polygon is closer to its generating point p_i than to any other p_j ($j \neq i$). The set of all the Voronoi polygons (or cells) is called a Voronoi diagram, as shown in Fig. 6. In order to generate such Voronoi diagrams, we choose to start from an initial periodic structure where the centers of the cells lie on a square grid with a period d, and we deform it. For that purpose, we randomly displace the cell centers according to a given statistical law. The new grid structure is defined as the Voronoi diagram obtained from the displaced cell centers. For example, in Fig. 7 we have represented different grid structures that correspond to different levels of disorder. They have been generated by displacing the cell centers so that each displacement in the x and the y direction is the realization of a uniform random variable in the interval $[-\alpha/2, \alpha/2]$. We define the deformation factor as follows:

$$a = \frac{\alpha}{d}. \tag{7}$$

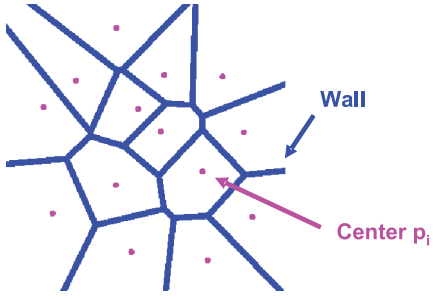

Fig. 6. (Color online) Illustration of a Voronoi diagram composed of Voronoi cells separated by walls. A Voronoi cell contains exactly one generating point p_i, and every point is closer to its generating point p_i than to any other p_j ($j \neq i$).

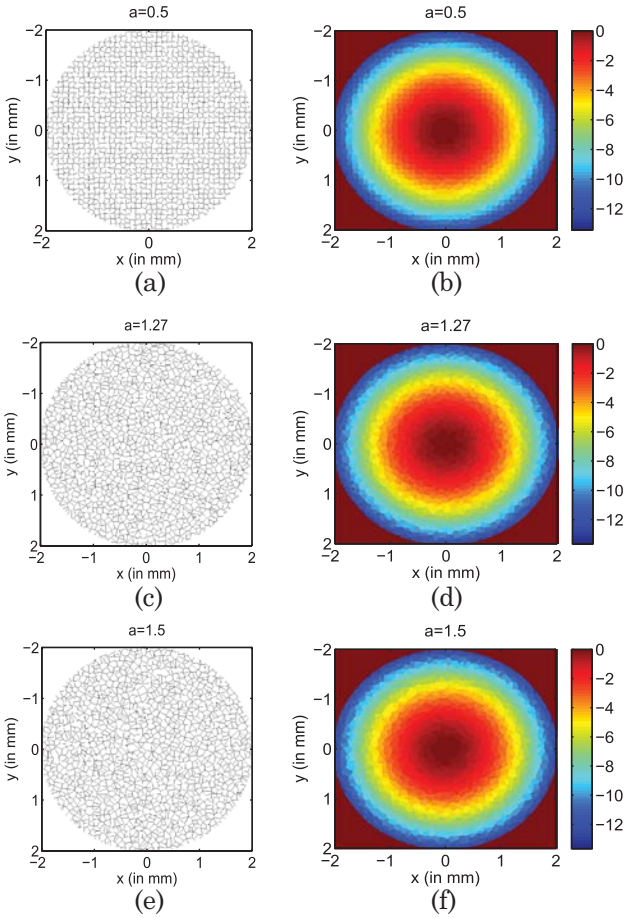

Fig. 7. (Color online) Increase of the randomness of the periodic distribution of centers, spaced every $d = 100\,\mu$m (Fig. 1). (a), (c), and (e) Associated Voronoi diagrams with walls only. Pupil diameter of 4 mm. The centers are moved according to a uniform distribution on a square of side a so that $a = 0.5$, $a = 1.27$, and $a = 1.5$. (b), (d) and (f) Corresponding Voronoi diagram correcting a $f = 2$ m lens.

The grids in Fig. 7 correspond to different values of a with $d = 100\,\mu$m. In this figure, we have also represented the corresponding phase profile when the SLM implements a lens of phase $\varphi_d(x,y)$ [see Eq. (1)] and focal length $f = 2$ m, sampled according to Eq. (4).

We have represented in Fig. 8 the two-dimensional angular distribution of the relative intensity in the focal plane for each modulator represented in Fig. 7, as well as a cross section in the horizontal direction. In Fig. 1(a), the grid is square-shaped with pixel pitch equal to $d = 100\,\mu$m. The grid structure represented in Fig. 7(a) corresponds to a small deformation of the square grid with a parameter $a = 0.5$. It is seen in Figs. 8(a) and 8(b) that the amplitudes of the higher-order peaks are reduced, especially those located at angles larger than 1°. On the other hand, a smooth scattered light distribution appears between the peaks. In the following, we shall call it the diffraction "halo."

It should be mentioned that a mean of 20 Voronoi simulations is shown in order to reduce the variance of the diffraction pattern and thus estimate more precisely the evolution of the higher-order peaks.

The grid structure represented in Fig. 7(c) corresponds to a larger deformation factor ($a = 1.27$). In the intensity distribution in Figs. 8(c) and 8(d), we see all the higher-order peaks have disappeared and the level of the halo has slightly increased. If a is further increased, as in Fig. 7(e) ($a = 1.5$), we see in Figs. 8(e) and 8(f) that the diffraction pattern remains quasi-identical.

In Fig. 9, we have plotted the evolution of the relative intensities of the order 0 and of the order 1 as a function of the deformation factor a. We notice that the order 1 decreases with a and then stabilizes to a constant value. This evolution is similar to what was observed in [9], where we have studied diffraction by the walls of the SLM (without phase function implemented). The only difference is that, in that case, after a first minimum for $a = 1.27$, the curve increases again (the first-order peak reappears) and reaches local minima around −60 dB for $a = l$ with l integer and $l \geq 2$. In the present case of pixels implementing a specific phase function, we have no local minima, as can be seen in Fig. 9, but the diffraction peak height saturates at some nonzero level, due to the halo, which increases as the focal length of the pixelated lens decreases. Even the location of the first minimum of the first-order peak is difficult to determine. To estimate it, we have used a ninth-order polynomial expansion for the first 40 values of the curve represented by a dotted line in Fig. 9. We obtain the estimated value $a = 1.26$ for a value of the first-order peak around −60 dB. We conclude that the evolution of the first-order is similar whether we consider the walls alone or the filled structure for $a \in [0, 1.27]$. A practical consequence of the results in Fig. 9 is that it is not necessary to distort the initial grid beyond $a = 1.27$: the relative intensity of the first-order peak does not decrease anymore.

As a result, we define the optimal Voronoi structure as the one obtained for $a = a_{\text{opt}}$. Since $a_{\text{opt}} = 1.27$, the optimal modulator structure is the same for the pixelated case and the walls only, which is very interesting in terms of technical design.

The value $a_{\text{opt}} = 1.27$ is obtained when the initial grid is square-shaped of size d and the cell centers are moved according to a uniform distribution on a square of side $\alpha = ad$. If one chooses another shape for the initial grid (for example hexagonal), or if one uses other statistics for the displacement of cell centers (e.g., uniform on a circle of radius $\alpha/2$ or Gaussian with standard deviation α), there is always a specific value a_{opt} of the deformation parameter $a = \alpha/d$, which is in general different from 1.27, that leads to the disappearance of the higher-order peaks. The Voronoi grids obtained for these optimal parameter values all have the same properties: uniform orientation of the walls and identical shape and level of the halo. We have not yet been able to find an analytical method to determine the value of the

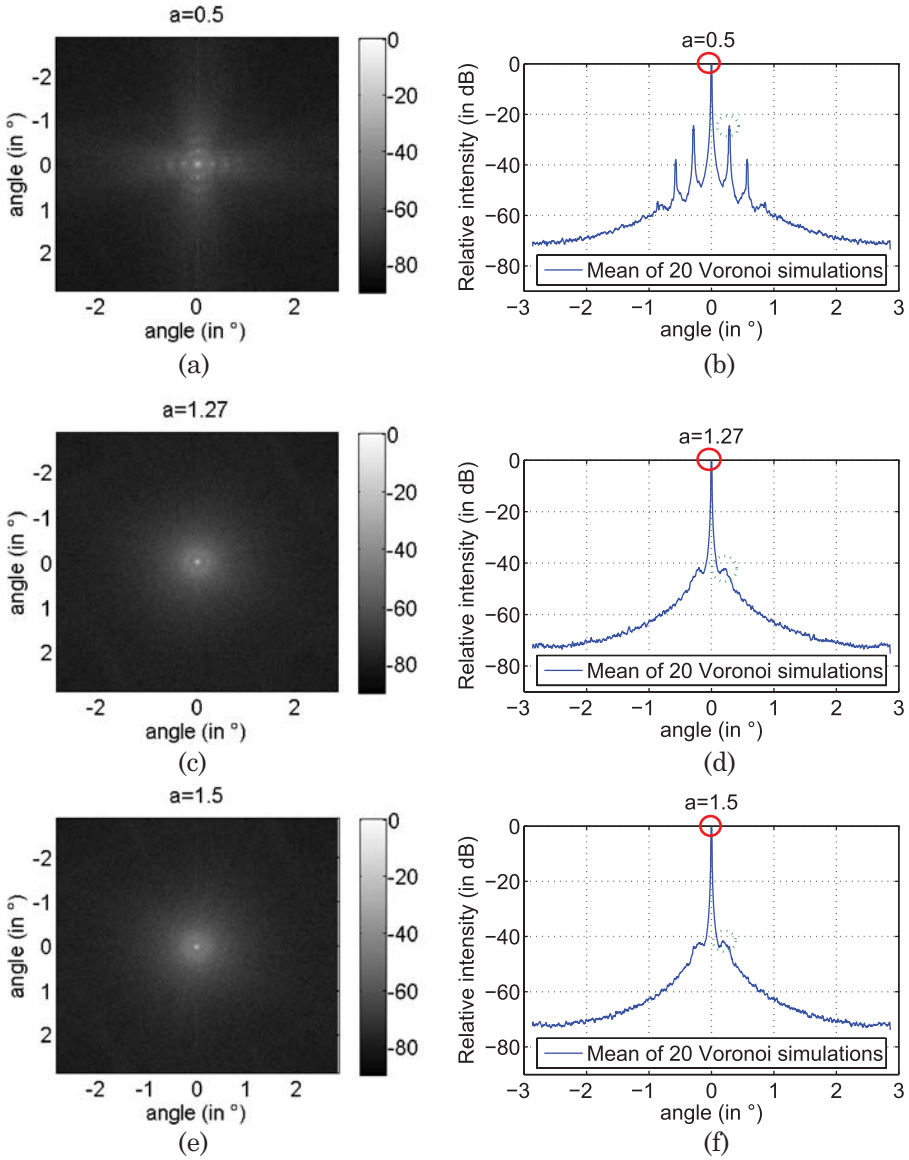

Fig. 8. (Color online) Diffracted intensity by the pixelated Voronoi components implementing a lens of focal length $f = 2$ in Fig. 7 and the corresponding cross section in the horizontal direction. (a), (b) $a = 0.5$. (c), (d) $a = 1.27$. (e), (f) $a = 1.5$. Pupil of 4 mm diameter.

optimal parameter, and we think that it is an interesting subject for further investigation.

In Fig. 5, we compare a horizontal section of the relative intensity diffracted by the regular square grid, the optimal Voronoi grid, and the isophases. First, we conclude that the optimal Voronoi structure is better than the square grid in spite of a lower Strehl ratio (Table 1) because the diffraction peaks vanish and the level of the halo is 18 dB lower. Secondly, we conclude that the isophase pixelation is the best choice in this situation because the isophases reduce the level of the diffraction halo 10 dB more than the Voronoi structure and the Strehl ratio is better (Table 1).

D. Conclusion

The method described in this paper is intended to reduce the diffraction peaks and to replace them by a halo. This is beneficial when SLMs are used for imaging purposes, when the point spread function includes the order 0 as well as the higher orders [13,14]. In general, if the scene has a smooth distribution of the luminance, the effect of pixelization on the resulting image will be low even if the pixels are periodically distributed, since the higher-order peaks are at least 10 dB below the zero order. On the other hand, when imaging bright pointlike objects on a dark background, like a streetlight by night observed through a periodic SLM prototype (see Fig. 10), higher-order peaks are well visible and the slight halo produced by Voronoi components would be visually much less annoying in this case.

We have investigated two techniques to reduce the diffraction peaks. We have shown that, in each case, it is possible to cancel the main unwanted diffraction peaks and essentially obtain a smooth diffraction halo by a suitable choice of parameters (γ for the isophases and a for Voronoi). As a result, the two

Fig. 9. (Color online) Evolution of the relative intensities of the order 0 and of the order 1 as a function of the parameter a for a pixelated lens of focal length $f = 2\,\mathrm{m}$ encoded on a Voronoi SLM. Average of the efficiencies on 20 realizations of two-dimensional Voronoi components.

techniques are better than a regular square SLM and are able to reduce the maximal unwanted light level to less than 50 dB below the signal peak. However, we have also shown that the isophases are better than the optimal Voronoi with a gain of 10 dB for the maximum level of the diffraction halo. In Section 3, we will compare these two techniques for wavefront correction in order to determine whether they are equivalent or not when other phase functions are implemented on the SLM.

3. Application to Wavefront Correction

The principle of wavefront correction is presented in Fig. 11. The idea is to correct a wavefront aberration with an SLM placed in the pupil of a perfect lens and illuminated by a monochromatic aberrated wave of

Fig. 10. (Color online) Night scene observed by a periodic pixelated prototype.

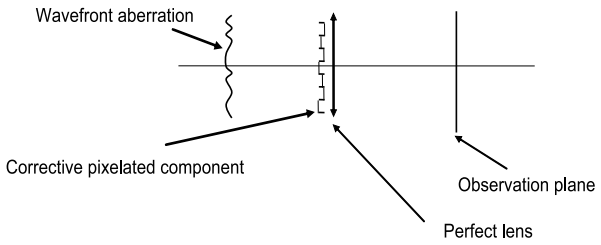

Fig. 11. Principle of wavefront correction.

wavelength $\lambda = 0.5\,\mu\mathrm{m}$ propagating parallel to the optical axis. We observe the distribution of light intensity in the focal plane, which is, in this simple case, the squared modulus of the Fourier transform of the modulator's transmittance. We shall consider the correction of astigmatism and coma wavefronts, which are interesting because their phase functions do not possess the rotational symmetry.

A. Correction of Astigmatism

Let us first consider the case of an astigmatism aberration corresponding to the following phase function:

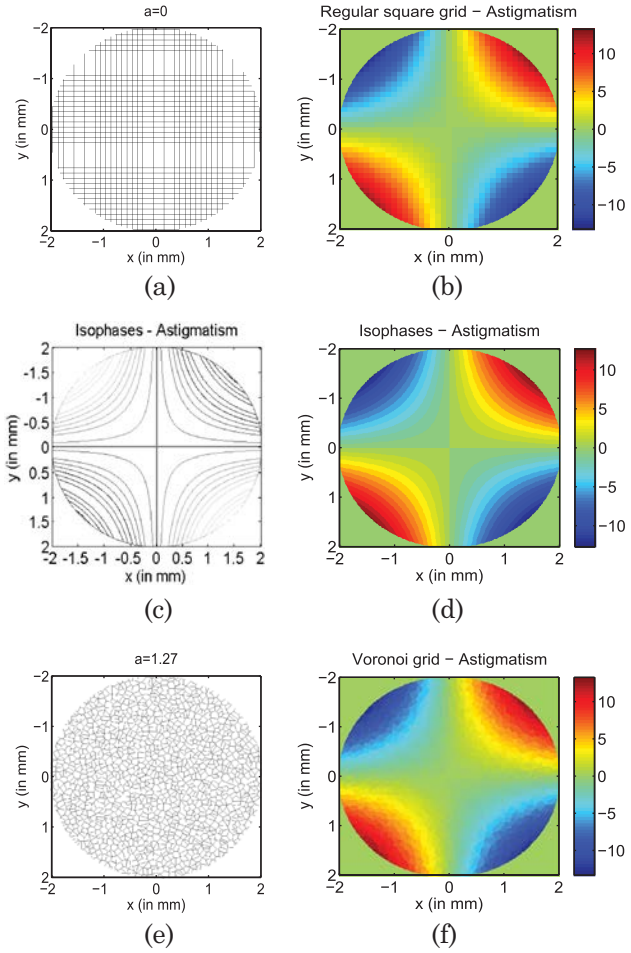

Fig. 12. (Color online) Structure of the pixelated modulators (first column) and the astigmatism wavefront encoded on them (second column). (a), (b) Regular square grid. (c), (d) Isophases. (e), (f) Optimal Voronoi grid.

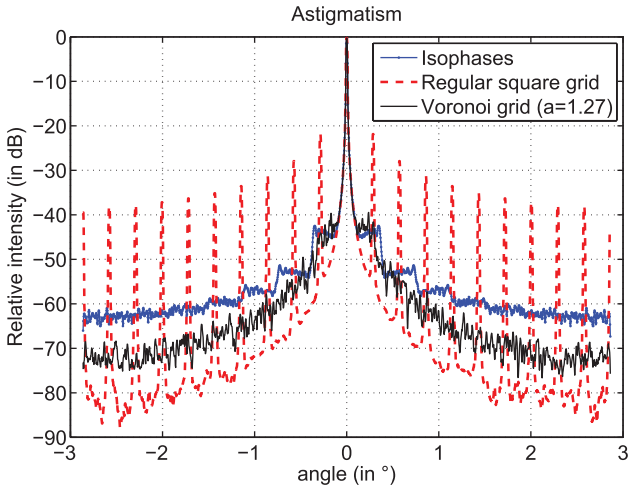

Fig. 13. (Color online) Correction of astigmatism. Comparison of the horizontal sections of the diffracted intensity by a regular square grid ($d = 100\,\mu$m), by an optimal Voronoi grid ($a = 1.27$), and by isophases.

$$\varphi_{\text{ast}}(X, Y) = 2A_{\text{ast}}XY. \tag{8}$$

We introduce the standardized variables (X, Y), such that $X = 2x/L$, $Y = 2y/L$, and $\sqrt{X^2 + Y^2} < 1$, where L is the pupil diameter. In order to have the same maximal slope value as in the case of the pixelated lens, we differentiate Eqs. (1) and (8), and, for $\lambda = 0.5\,\mu$m and $f = 2\,$m, we obtain $A_{\text{ast}} = 4\pi$. In Fig. 12, we present the structure of the SLMs pixelated with the regular grid, with the isophases, and with the Voronoi techniques, and the phase function encoded on them. For the isophases, we choose the optimal γ so that $\gamma = 0.15$ and we use the same optimal Voronoi structure as the lens (see Subsection 2.C). We represent, in Fig. 13, a cross section of the relative intensity diffracted by each SLM. The chosen direction is the horizontal one, where the first-order peak is maximum.

As for the pixelated lens of Subsection 2.C, we first conclude that the optimal Voronoi structure is preferable to the square grid in spite of a lower Strehl ratio (Table 2) because the diffraction peaks vanish and the level of the halo is 18 dB lower. Second, we conclude again that the isophase pixelation is the best choice in this situation because the isophases reduce the level of the diffraction halo 4 dB more than the Voronoi structure and the Strehl ratio is better (Table 2).

Table 2. Correction of Astigmatism[a]

	S	G
Square grid	0.94	-
Isophases	0.93	22
Voronoi ($d = 100\,\mu$m)	0.92	18

[a]Strehl ratios S and difference in dB, denoted G, between the first-order peak of the square grid and the maximum of the halo of the studied pixelated grid.

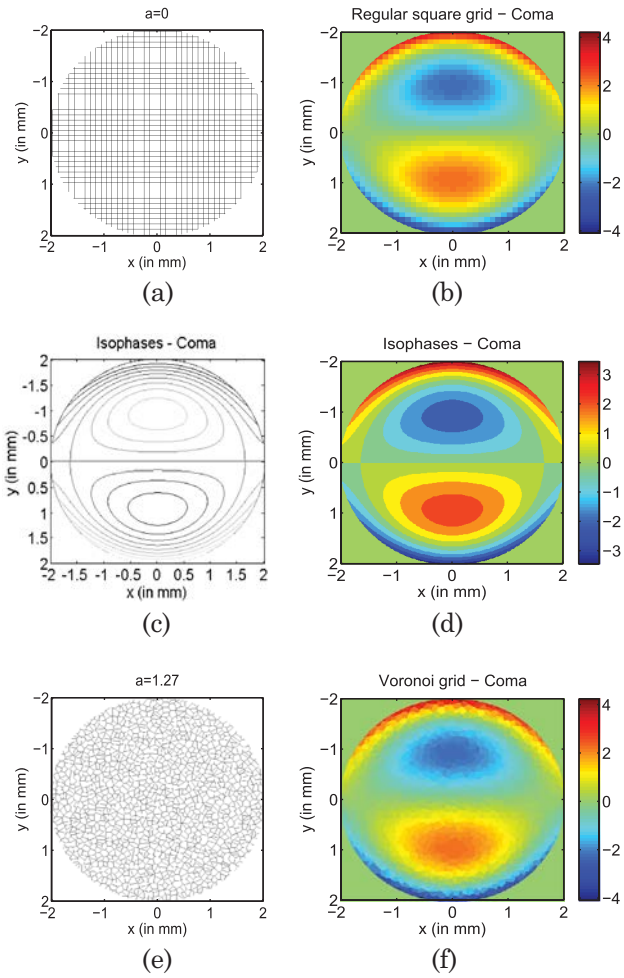

Fig. 14. (Color online) Structure of different pixelated modulators (first column) and the coma wavefront encoded on them (second column). (a), (b) Regular square grid. (c), (d) Isophases. (e), (f) Optimal Voronoi grid.

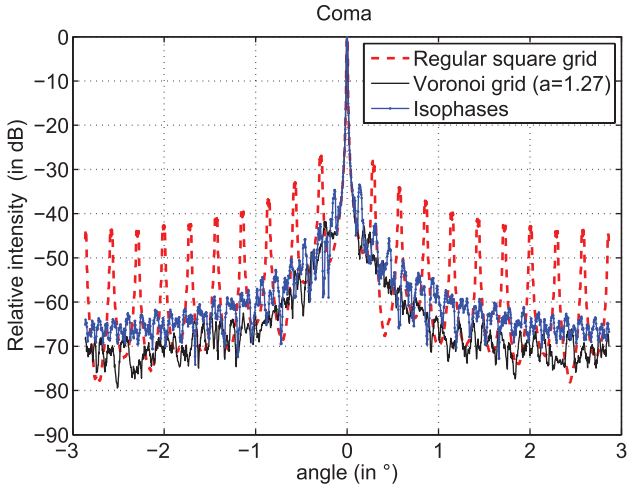

Fig. 15. (Color online) Correction of coma. Comparison of the vertical sections of the diffracted intensity by a regular square grid ($d = 100\,\mu$m), by an optimal Voronoi grid ($a = 1.27$) and by isophases.

Table 3. Correction of Coma[a]

	S	G
Square grid	0.98	-
Isophases	0.98	8
Voronoi ($d = 100\,\mu$m)	0.97	15

[a]Strehl ratios S and difference in dB, denoted G, between the first-order peak of the square grid and the maximum of the halo of the studied pixelated grid.

B. Correction of Coma

We will now study the case of a coma that corresponds to the following phase function:

$$\varphi_{\text{coma}}(X,Y) = A_{\text{coma}}(-2Y + 3Y^3 + 3X^2Y). \quad (9)$$

In order to have the same maximal slope value as in the case of the pixelated lens, we differentiate Eqs. (1) and (9), and, for $\lambda = 0.5\,\mu$m and $f = 2$ m, we obtain $A_{\text{coma}} = \frac{8\pi}{7}$. In Fig. 14, we present the structure of the SLMs pixelated with the regular grid, with the isophases, and with the Voronoi techniques, and the phase function encoded on them. For the isophases, we choose the optimal γ so that $\gamma = 0.1$, and we use the same optimal Voronoi structure as for the lens and the astigmatism (see Subsection 2.C). We represent, in Fig. 15, a cross section of the relative intensity diffracted by each component. This time, the chosen direction is the vertical one, where the first-order peak is maximum.

First, we notice that the optimal Voronoi structure is better than the square grid because the diffraction peaks vanish and the level of the halo is 15 dB lower, whereas the Strehl ratio has the same value (Table 3). Second, we point out that it is also better than the isophases, which only lead to a reduction of the level of the diffraction halo of 8 dB for an essentially identical Strehl ratio. This fact can be understood by looking at Fig. 16, where the vertical profile of the coma phase function is represented. Between [−1 mm, 1 mm], this function is a straight line, which means that, when we slice the three-dimensional curve with planes $z = 2\pi\gamma$, the intervals between two isophases are the same. This introduces a periodicity that is at the origin of diffraction peaks visible in Fig. 15. On the other hand, with the Voronoi structure, there is no periodicity and thus no diffraction peak. In this situation, the Voronoi technique is thus the best choice.

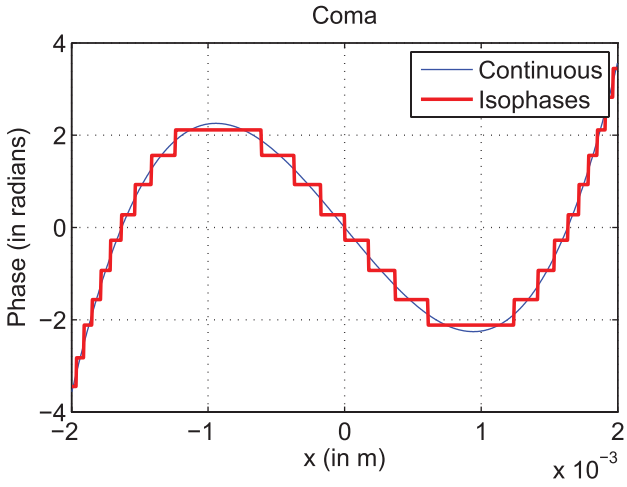

Fig. 16. (Color online) Comparison of the continuous and isophase profiles of the coma.

C. Conclusion

By considering two phase functions without rotational symmetry, we have shown that it was possible to minimize the diffraction peaks, and essentially obtain a pure diffraction halo by a suitable choice of parameters for both pixelation techniques. We have demonstrated that each pixelation technique behaves differently depending on the phase function. With the isophase method, the amount of reduction of the first-order peak depends heavily on the encoded phase function. In unfavorable cases, such as coma, this reduction may be insufficient. On the other hand, the Voronoi method has a much more stable behavior with respect to the encoded phase.

4. Conclusion

As a summary, pixelated diffractive optical elements used for wavefront shaping suffer distortion due to the sampling operation itself. In this paper, we have investigated a new, nonperiodic pixelation technique derived from the Voronoi tesselation method. Extending our previous work, where only the Voronoi pixel walls were considered, we have shown that it is effective to avoid the far-field diffraction peaks that occur with periodic sampling. In the cases considered, at a moderate cost in terms of Strehl ratio, and with a proper selection of the parameter to generate the Voronoi map, the diffraction peaks are completely suppressed at the expense of a modest halo. To implement wavefront shaping on an SLM, the method is therefore fairly attractive. On the other hand, if the aberration is known, no active wavefront shaping method is required. In that case, if the fabrication method involves fixed phase pixels, at least for some wavefront shapes, the isophase method may provide better results in that it cancels the far-field diffraction peaks at a lower cost in terms of halo buildup.

The present paper was entirely devoted to the design of structures. The problem of their practical realization remains to be addressed. A possible way of solving it could be using photolithographic equipment, and some real devices are under realization with this technology. An in-depth study of this issue is an interesting topic for future work.

References

1. D. M. Cottrell, J. A. Davis, T. R. Hedman, and R. A. Lilly, "Multiple imaging phase-encoded optical elements written as programmable spatial light modulators," Appl. Opt. **29**, 2505–2509 (1990).

2. R. B. Apte, F. S. A. Sandejas, W. C. Banyai, and D. M. Bloom, "Deformable grating light valves for high resolution displays," presented at the Solid-State Sensor and Actuator Workshop, Hilton Head, S.C., USA, 1994.
3. S. Esener, J. L. Horner, and K. M. Johnson, eds., feature on Spatial Light Modulators, Appl. Opt. 31 (20) (1992).
4. A. L. Lentine, J. N. Lee, S. H. Lee, and U. Efron, eds., feature on Spatial Light Modulators, Appl. Opt. 33 (14) (1994).
5. E. Carcolé, J. Campos, I. Juvells, and S. Bosch, "Diffraction efficiency of low-resolution Fresnel encoded lenses," Appl. Opt. **33**, 6741–6746 (1994).
6. E. Carcolé, J. Campos, and S. Bosch, "Diffraction theory of Fresnel lenses encoded in low-resolution devices," Appl. Opt. **33**, 162–174 (1994).
7. E. Carcolé, J. Campos, I. Juvells, and J. R. de F. Moneo, "Diffraction theory of optimized low-resolution Fresnel encoded lenses," Appl. Opt. **34**, 5952–5960 (1995).
8. M. Peloux, P. Chavel, F. Goudail, and J. Taboury, "Shape of diffraction orders of centered and decentered pixelated lenses," Appl. Opt. **49**, 1054–1064 (2010).
9. C. Benoit-Pasanau, F. Goudail, P. Chavel, J. P. Cano, and J. Ballet, "Minimization of diffraction peaks of spatial light modulators using Voronoi diagrams," Opt. Express **18**, 15223–15235 (2010).
10. A. Maréchal, "Etude de l'éclairement au centre de la tache de diffraction dans le cas de diverses aberrations géométriques," C. R. Hebd. Séances Acad. Sci. **218**, 395–397 (1944).
11. M. Born and E. Wolf, *Principles of Optics: Electromagnetic Theory of Propagation, Interference, and Diffraction of Light*, 7th ed. (Cambridge University, 1999).
12. G. F. Voronoi, "Nouvelles applications des paramètres continus à la théorie des formes quadratiques," J. Reine Angew. Math. **1908**, 198–287 (1908).
13. F. Diaz, F. Goudail, B. Loiseaux, and J.-P. Huignard, "Increase in depth of field taking into account deconvolution by optimization of pupil mask," Opt. Lett. **34**, 2970–2972 (2009).
14. S. Sherif, T. Cathey, and E. Dowski, "Phase plate to extend the depth of field of incoherent hybrid imaging systems," Appl. Opt. **43**, 2709–2721 (2004).